

The Effect of Anisotropic Interactions Strength on Glass Transition in Single Component System: A Computational Study

Author: Itay Schachter

Amirim Adviser: Prof. Daniel Harries

25th September 2019

ברצוני להודות לפروف' דניאל הריז על סיועו בעבודה זו ובכלל
כמנחה ומנטור ובחשיפתי לתחומיים רבים ומעניינים,
ולבת זוגי סופי על תמיכתה הרבה וחיזוקיה במהלך הפרויקט
והתואר בכלל.

Contents

I	Introduction	4
II	Theory of Glass Transition	6
1	Mode Coupling Theory for Supercooled Liquids	6
2	Random First Order Theory of The Mosaic State	8
3	Relevant Glass Transition Indicators	9
3.1	Heat Capacity Near The Glass Transition	9
3.2	Point-to-Set (PTS) Correlation Length	10
4	Other Measured Sizes	11
4.1	Pressure	11
4.2	Heat Capacity	11
4.3	Entropy	11
4.4	Free Energy	11
4.5	Radial Distribution Function	12
4.5.1	Potential of Mean Force (PMF)	12
III	Computational Methods	13
5	Simulation Methods	13
5.1	The Metropolis-Hastings Algorithm	13
5.2	Advanced Monte Carlo Techniques	14
5.2.1	Swap Monte Carlo	15
5.2.2	Parallel Tempering	15
5.2.3	Generalization to the Isobaric-Isothermal Ensemble	16
6	Analysis Methods	16
6.1	Implementation of PTS Correlation Length	17
IV	Simulation Details and Results	18
7	The Final Model	19
8	Failed Trials and Conclusions	21
9	Simulation Details - The Final Model	23
10	Results and Discussion	24
10.0.1	Standard Thermodynamic Sizes	24
10.0.2	Radial distribution Functions and Structure	27
V	Summary	36
VI	Appendixes	37
11	Appendix A: Ising Model Simulations and Results	37
VII	References	39

Part I

Introduction

Most people know about three states of matter (gas,liquid,solid).As shown by van der Waals that the gas and liquid states are a continuum and only differ quantitatively[1],and both are qualitatively differ from crystalline solid state,which have an ordered,periodic structure and also very rigid.

Glass is defined as amorphous solid,as so,without long-range order in the molecular level,which is also a property of the liquid state.

In principle, to obtain glass, one has to cool a liquid under its melting point (without crystallization-which is avoidable when cooling fast enough to suppress nucleation and growth of nuclei).Under the m.p. the liquid is called *supercooled liquid* which is meta-stable with respect to the crystalline state.As one keeps cooling the liquid (at the rate of ν) he would see that the relaxation time τ (can be related to viscosity) of the liquid extends until it vanishes (and the viscosity diverge) at the calorimetric glass transition temperature T_ν .This change is called the glass transition,at which the supercooled liquid falls out of (meta-stable) equilibrium, this transition includes a small “bump” in the heat capacity of the glass and below T_ν the heat capacity gets below that of the supercooled liquid. T_ν depends on the cooling rate and monotonically decreases with it.As so,the definition of the *glass transition temperature* (T_g) is the *range* of temperatures in which the supercooled liquid exhibits glass transition.As $\nu \rightarrow 0$ (i.e. infinitely slow cooling) we obtain that $T_\nu \rightarrow T_0 > 0K$ (can be obtained via extrapolation).This temperature can be related to the *Kauzmann temperature* T_K under which an ideal glass ($\nu \rightarrow 0$) should have smaller entropy then the crystalline state(which is paradoxical[2]).An empirical relation shows that $T_0 \approx T_K$ for some glass formers[3],which hints a thermodynamic basis to the glass transition (as a way for the system to escape from the paradox by falling out of equilibrium).

The glass transition seems as continuity with the supercooled liquid (in terms of properties of the system- e.g. volume,heat capracity),unlike the liquid-solid transition.I should note that in contrary to liquid-solid transition the glass transition is not a thermodynamic phase transition, as it is not a change between 2 equilibrium phases and also notably dependent on the dynamics.As glass transition depends on preparation history,so does the properties of the glass (e.g. volume,strength).

A key property of glasses is non-ergodicity – which means that the system is stuck in a partial region of the states space in comparison to the ones that are accessible for the (bit warmer) supercooled liquid.This property is connected to the hysteresis of such system.

For a material to be a good glass former, it should have a molecular-level tendency to geometrically frustrated structures (e.g.:long chained polymers, SiO_2).As a result, the crystallization is suppressed and amorphous state is reachable.

As noted above, glass transition seems to have both kinetic and thermodynamic basis and as one might expect, theories of glass transition falls into one of those two categories[4].

There are some theoretical models for frustrated (not necessarily geometrically) systems.One of those is the *Ising model* with 2D Hexagonal lattice and anti-ferro interactions in which particles are placed on a lattice and have a spin (up or down) and the interaction are with their nearest neighbors, it turns out that there is no apparent order for the equilibrium state, as described on Appendix A.

For many-particles computer simulations can be used to get a system that have a glass transition.One method is to take multi-component system of spherical particles with varying radius – which with the right parameters don't tend to crystallize (e.g.[5]).There are also examples for glass transition for single-component system, with some kind of anisotropy, for example at systems with dipole interactions (e.g.[6]).

There are some possible methods in order to check if a system is in the glassy state or getting close to the glass transition (e.g.:change of some characteristic lengthscale). Some of them are only possible at a Molecular Dynamic simulation (as the glass transition is characterized by divergence of dynamical properties of the system) and others can be examined in Monte-Carlo simulation.

The main goal of this work at the academic level is to explore the effect of anisotropic interactions in different levels of strength on the crystallization and glass transition of a single-component system. As such, the main parts of the project was:

1. to find a fitting potential for the particle with simple anisotropic magnitude parameter which actually doesn't crystallize when the anisotropy is strong enough.
2. running of the simulations and analysis.

The goals of this work at the educational level were to learn about Monte Carlo simulations and write one from scratch via Python, and also getting to know and using modern methods in the fields of computational simulations and glassy systems.

At Part II of the work I'll describe some of the theory behind glassy state, glass transition and some measurable quantities to follow it. At Part III I'll describe the computational methods behind the simulation and the related theory. At Part IV I'll give the precise details of the simulations and the analysis results, and would also briefly describe previously failed potential results. At Part V I'll give a summary to this project. Part VI contains the appendixes.

Part II

Theory of Glass Transition

In this part I'll describe some ideas in the theory behind glassy state and glass transition and will build a necessary vocabulary to talk about this phenomena at my simulations.

Some (subjectively) brief notes:

Conventions

- By default $k_B = 1$

Strong and Fragile Glasses There is a note that need to be made about this subject, as in the simulations we began with a fragile (and bad) glass-former and with the increasing strength of the anisotropic interactions the particles will become more network formers. So, experimentally[10], strong glasses relaxation time have an Arrhenius behavior at $T > T_g$ while fragile glasses tend to have non-Arrhenius behavior of the relaxation time and tend to be fitted in first approximation by Vogel-Fulcher law: $\tau = \tau_0 e^{\frac{DT_0}{T-T_0}}$ with τ_0 being pre-exponential coefficient, D is the fragility coefficient and T_0 is the temperature described above, a more detailed explanation is given at Section 2. Strong glass-formers are network formers via strong bond (such as $\text{SiO}_2, \text{GeO}_2$) in contrast to fragile glasses.

α and β Relaxation Processes The dynamics of a deeply supercooled liquid can be detailed by two different types of movement: slow collective and fast non-collective. The relaxation itself occurs due to both, and each corresponds to a different relaxation process. The first to the slow α relaxation process and the second to the fast β relaxation process. Those 2 relaxations can be measured in the vicinity of T_g from each other experimentally (as in [13], at the beginning only the β relaxation is really pronounced as they differ by scale of ~ 5) where the β relaxation have an Arrhenius behavior and the α relaxation time diverge at T_g and can be fitted by VF law.

The Adam-Gibbs Relation Adam and Gibbs theory [20] describes the increasing relaxation time with the supercooling of liquid which includes the participation of growing cooperative rearranging regions. In the theory, the cooperative rearranging regions are characterized by a typical length r which is defined by regions with few (some constant number) accessible configurations of which the entropy density obeys $s_c(T) \propto r^{-3}$ (as each region correspond to low number of configurations). If we assume that τ of cooperative movement of the size r obeys Arrhenius behavior with energy barrier $\Delta \propto r^3$ it results with $\tau = \tau_0 e^{\frac{\text{const}}{T s_c(T)}}$ which is the Adam-Gibbs relation for relaxation time.

I'll note that this relation connects the diverging viscosity to the vanishing entropy at T_K , thus relates the Kauzmann paradox to the critical slowdown.

1 Mode Coupling Theory for Supercooled Liquids

In this section we mainly discuss the mode-coupling theory for *simple* liquids which are isotropic unlike the final model's potential which is (increasingly) anisotropic and have some weak behavior of network forming. But the results of the theory should apply (at least) qualitatively to the model if glass transition is

reachable[9], it should be noted that there are some extended mode coupling theories that can be applied to anisotropic particles[12].

I'll also note that the mode-coupling theory is a dynamic view of the glass transition.

When mode-coupling theory was first applied to supercooled liquids it viewed the glass transition as a transition from ergodic to non-ergodic in the relaxation dynamic of volume fluctuations[7]. The non-ergodicity is due to structural arrest of the glass which arises from the solution of an evolution equation of the volume fluctuations. In later works the model was generalized to the dynamics of other relaxation processes (i.e. other time correlation functions)[8].

For simplicity I'll show the main points in the development of the mode-coupling theory for the density fluctuations case[9, 4].

Let the van Hove density-density correlation function

$$G(\mathbf{r}, t) = \rho^{-1} \langle \rho(\mathbf{r}, t) \rho(\mathbf{0}, 0) \rangle$$

when represented by its Fourier transform:

$$\begin{aligned} F_{\mathbf{k}}(t) &= N^{-1} \langle \rho_{\mathbf{k}}(t) \rho_{-\mathbf{k}}(0) \rangle = \int G(\mathbf{r}, t) e^{-i\mathbf{k} \cdot \mathbf{r}} d\mathbf{r} \\ \rho_{\mathbf{k}} &= \int \rho(\mathbf{r}) e^{-i\mathbf{k} \cdot \mathbf{r}} d\mathbf{r} = \sum_i e^{-i\mathbf{k} \cdot \mathbf{r}_i} \end{aligned}$$

the static structure factor is defined as $S_{\mathbf{k}} = F_{\mathbf{k}}(0)$ and we shall define $\Phi_{\mathbf{k}}(t) = F_{\mathbf{k}}(t)S_{\mathbf{k}}^{-1}$ as Φ obeys the differential equation:

$$\ddot{\Phi}_{\mathbf{k}}(t) + \nu_0 \dot{\Phi}_{\mathbf{k}}(t) + \Omega_{\mathbf{k}}^2 \Phi_{\mathbf{k}}(t) + \int_0^t \Gamma(t-t') \dot{\Phi}_{\mathbf{k}}(t') dt' = 0$$

with initial conditions: $\Phi_{\mathbf{k}}(0) = 1, \dot{\Phi}_{\mathbf{k}}(0) = 0$ where Γ is a memory function, ν_0 a damping constant and $\Omega_{\mathbf{k}}$ a characteristic frequency.

The solutions of the equation above vary for different volumes and temperatures, by their decay behavior we define:

$$\begin{aligned} \lim_{t \rightarrow \infty} \Phi_{\mathbf{k}}(t) &= 0 \text{ ergodic} \\ \lim_{t \rightarrow \infty} \Phi_{\mathbf{k}}(t) &= f_{\mathbf{k}} \neq 0 \text{ non-ergodic} \end{aligned}$$

where $f_{\mathbf{k}}$ is called *the non-ergodicity parameter*. The theory predicts that for non-ergodic system we obtain:

$$\frac{f_{\mathbf{k}}}{1 - f_{\mathbf{k}}} = \Gamma_{\mathbf{k}}(t \rightarrow \infty)$$

so, we define a supercooled liquid if Φ decays to 0 and otherwise a glassy state.

The theory yields that for a small change in (ρ, T) we could get a sharp change from ergodicity to non-ergodicity and therefore a glass transition.

Our main interest on the mode-coupling theory for the current project is for the deep supercooled liquid region in the vicinity of the glass transition.

We'll define (ρ_x, T_x) as the temperature and density of the structural arrest (in the sense that mode-coupled relaxation time diverges, but activation-based relaxation is still available and may restore ergodicity to the system). The mode-coupling theory predicts that for $T > T_x$ in a high enough region the viscosity $\eta \propto (T - T_x)^{-\gamma}$ with $\gamma > 0$, at a lower temperature region near T_x the behavior is approximately Arrhenius or VF law (as activation-based relaxation dominates under T_x). Another important result of MCT under the

two-mode approximation that near T_x the relaxation is two-stepped, there are two characteristic times τ_I, τ_{II} that indicate the power law of the decay, as for $t_0 \ll t \ll \tau_I$ (t_0 is a microscopic characteristic time) the long-time decay is:

$$\Phi_k(t) - f_k \sim \begin{cases} \left(\frac{t}{\tau_{II}}\right)^{-a} & t \ll \tau_{II} \\ \left(\frac{t}{\tau_{II}}\right)^b & t \gg \tau_{II} \end{cases}$$

where $b, a > 0$ and both are obtained from the solutions to some equation that relate to characteristic lengthscale of the system. (more details at [9]).

It also should be noted that the 2 relaxation rates of Φ_k aren't of the α and β relaxation processes.

As I mentioned above - in this project, our particles interactions become increasingly anisotropic. I think it would be an interesting Idea for a future research to actually try a check for a two-stepped relaxation as we increase the anisotropy, as it was found at [11] that there are strong glasses that have a similar two-stepped relaxation.

2 Random First Order Theory of The Mosaic State

The theory of Random First Order Theory (RFOT) is a thermodynamically-based theory that was developed in order to describe the glass transition.

The theory presented in this chapter describes fragile glasses as the VF behavior of the viscosity could also be described by an energy barrier that increases as $T \rightarrow T_0^+$, which suggests the rise of an "amorphous order" at low temperatures where collective movements of increasing number of particles (as function of T) are needed to restore ergodicity to the system[14].

In the theory one treats the glassy state as a separate state of matter, also one expects a very large number of meta-stable glassy states[15]. Also, the glassy state can be described by some (maybe unknown) order parameter that depends on spatial fluctuations of some sort, each glassy state has different order parameter as one might expect and it changes discontinuously at T_g . The glass transition and is described by two distinct transitions (as can be seen in some mean field spin models and mean field approximation of liquid state models [15]). The first transition is the *dynamic transition* at $T_d > T_K$ under which there is large number of similar uncorrelated states with zero overlap (the state space has many disconnected -by some barrier- minima). At $T \in (T_K, T_d)$ for each separate state α of the system we'll denote the free energy as F_α and the canonical free energy F_c of the system can be described by:

$$Z = e^{-\beta F_c} = \sum_{\alpha} e^{-\beta F_{\alpha}}$$

as the system minima are disconnected F_c is not a true physical free energy. F_c can be related to the component average free energy \bar{F} of the system via:

$$\bar{F} = \sum_{\alpha} P_{\alpha} F_{\alpha}, P_{\alpha} \stackrel{1}{=} \frac{1}{Z} e^{-\beta F_{\alpha}} \implies F_c = \bar{F} + T \sum_{\alpha} P_{\alpha} \ln P_{\alpha} = \bar{F} - TS_c$$

1: right under the assumption that the liquid is cooled to (and under) T_d slow enough to be at equilibrium - so it could fall to one of the states in the equilibrated probability.

where S_c is the configurational entropy of the system. \bar{F} is the physical free energy of the system, as it doesn't include the entropy gain from states which are inaccessible during finite-time observation. This transition is related to the mode-coupling theory (as such under T_d activated movements are still present) and the *dynamic heterogeneity* of the glassy-like state is described by the multiple states under T_d . The second transition is

called the *Kauzmann transition* (referred to as the random first order transition) and it's the one we're more familiar with, which at T_K where the entropy of the system vanishes (and thus the activated transport through states).

We'll now describe the transfer from state α to state β (at $T \in (T_K, T_d)$) by the *mosaic state* model, as somewhat analogous to nucleation. We'll freeze the particles outside of a sphere of radius R at the supercooled liquid state, and we'll call the initial state of the sphere as α . If the system would change its state to different state $\gamma \neq \alpha$ we can safely assume that there is a mismatch with the amorphous boundary conditions and so a penalty of $\Upsilon_{\alpha,\gamma} R^\theta$ (with $0 < \theta \leq d - 1$ as $d = 3$ the dimension of the system an exponential scaling coefficient), we'll also assume that $\Upsilon_{\alpha,\gamma}$ doesn't fluctuate much and as so $\Upsilon_{\alpha,\gamma} \approx \Upsilon_0$ and so the partition function of the sphere is:

$$Z_\alpha(R, T) = e^{-\frac{\Omega R^3 f_\alpha}{T}} + \sum_{\gamma \neq \alpha} e^{-\frac{\Omega R^3 f_\gamma + \Upsilon_0 R^\theta}{T}} \approx e^{-\frac{\Omega R^3 f_\alpha}{T}} + \int_{f_{min}}^{f_{max}} e^{-\frac{\Omega R^3 [f - T\sigma(f, T)] + \Upsilon_0 R^\theta}{T}} df$$

where $\Omega = \frac{4\pi}{3}$ and $\sigma = \ln \mathcal{N}$ with \mathcal{N} the number of states of free energy f at T , and σ is the entropy density as function of free energy and temperature. Under the assumption that there is a typical free energy f^* and σ^* which is more significant from the other free energies for that temperature the partition function is almost independent of α :

$$Z(R, T) \approx e^{-\frac{\Omega R^3 f^*}{T}} \left(1 + e^{\Omega R^3 \sigma^* - \frac{\Upsilon_0 R^\theta}{T}} \right)$$

So the dependence on R of the partition function (and as result the number of available states) is exponentially large, and for some ξ if $R < \xi$ there is essentially one meta-stable state (α) of the system (i.e. non-ergodicity as in glass, even for $T > T_K$) and if $R > \xi$ there are enough meta-stable states available to the system (and α becomes unstable) and we obtain "entropic melting" of the cavity. This ξ is the typical length scale of the mosaic state[16] and also define the maximal scale in which it's reasonable to define a meta-stable state (as each state is unstable when ergodicity is restored). As one can see: $f(R \gg l^*) \approx f^*(T) - T\sigma^*(T) + O(l^{*\theta-d})$ which is in agreement with the relation between F_c and \bar{F} that we described above. One can interpret this result of mosaic state roughly as a typical size of "glass fragment" on which the supercooled liquid is built from, as analogy to crystallites in poly-crystals.

3 Relevant Glass Transition Indicators

3.1 Heat Capacity Near The Glass Transition

In this sub-section I'll describe the behavior of entropy and heat capacity before and after the glass transition. By Clausius equality $dS = \frac{dq}{T}$ and for quasi-static isobaric cooling $dS = \frac{C_p}{T}dT$, so the *excess entropy* of the supercooled liquid (in comparison to the crystal state) for T_m : $\Delta S(T_m) = \frac{\Delta H_m}{T_m}$ and for $T < T_m$ is:

$$\Delta S(T) = \Delta S(T_m) - \int_T^{T_m} \frac{C_{p,liquid} - C_{p,crystal}}{T'} dT' = \frac{\Delta H_m}{T_m} - \int_T^{T_m} \frac{\Delta C_p}{T'} dT'$$

as $\Delta C_p > 0$ and can be approximated and extrapolated nearly as a constant (so $\Delta S(T) \cdot T$ is linear)[17] so we get the Kauzmann paradox where for $T < T_K$ $\Delta S(T) < 0$. This result is not reasonable as supercooled liquid would obtain negative entropy under some temperature as $S_{crystal} \xrightarrow{T \rightarrow 0K} 0$. As in reality the relaxation rate vanishes when $T \rightarrow T_0 \approx T_K$ it is impossible to cool down the meta-stable supercooled liquid without falling out of equilibrium and we obtain a real glass with $C_{p,glass} \approx C_{p,crystal}$ (as the glass behaves as amorphous solid), and the Kauzmann paradox is avoided. So, the heat capacity jumps at T_ν which is measurable in experiments and simulations when the simulation reached metastability/equilibrium.

3.2 Point-to-Set (PTS) Correlation Length

In Section 2 we've discussed the RFOT of the mosaic state, in particular about the typical (static - time independent) lengthscale ξ which we'll now describe how to obtain via measurement of the decay rate of a relevant point-to-set correlation[19, 16, 18].

As in the mosaic state thought experiment, lets freeze all the system beside a ball of a radius R with. In the middle of the sphere we'll take a box with sides in constant length $L < R$ and divide it to N_i small enough boxes of equal volumes l^3 so each box could physically contain only one particle at a time. We'll now define the function $n_i(t)$ which counts the number of particles in box i at time t ($n_i(t) \in \{0, 1\}$) and lets define a collective overlap function between the initial state $t = 0$ to a later state at some time t :

$$q(t, R) = \frac{\sum_i \langle n_i(t) n_i(0) \rangle}{l^3 N_i \cdot \rho} \quad q(R) := q(t \rightarrow \infty, R)$$

Also $q(0, R) = 1$ and if the system got to totally uncorrelated states q would be equal to $q_0 = l^3$. Apparently the (roughly speaking) decay length of $q(R)$ with $R \rightarrow \infty$ is a characteristic lengthscale ξ' which can be related to the point-to-set correlation length [22] that is described below. The method of extraction of ξ' for the MC simulations is given at Part III.

After we've defined a relevant relaxation time for our system we can discuss its expected behavior as a function of R . As we've seen at Section 2 the configurational entropy of the sphere competes with the surface tension. As we've assumed for the Arrhenius behavior of τ in the AG relation we'll assume here that the energy barrier for the relaxation of a sphere of radius R obeys $\Delta \propto R^\psi$ for some $\psi \leq 3$.

When $R < \xi$ the relaxation can't restore ergodicity and the system is stuck at the initial state as the entropy of the sphere is small, as such, there is a relatively small set of available configurations of the system that can be access and those are accessible by mostly non-collective movements and i.e. dictated by the β relaxation rate. But as $R \rightarrow \xi$ more collective movements are available and the relaxation rate will be shifted toward the α relaxation rate (also the relaxation time grows with the energy barrier). On the other hand, for $R > \xi$ ergodicity is restored and the system have many meta-stable states accessible so the decorrelation can only occur by collective movements of the size ξ or bigger and thus the relaxation depends on collective movements of "sub-cavities" of that size. As collective movements of the size bigger than ξ become significantly slower than those of the size ξ we find that the relaxation time is about $\tau(R) = \tau(\xi)$. When taking $R \rightarrow \infty$ we'll also obtain that the bulk relaxation time is $\tau_{bulk} = \tau(R \rightarrow \infty) = \tau(\xi)$. So, by finding the sphere size at which τ stabilize to a constant would give us ξ .

We also need to address the behavior of ξ when $T \rightarrow T_K$, naively (and correctly) one would expect the $\xi \rightarrow \infty$ as the configurational entropy goes to 0, particularly in spheres of finite volume. The more rigor proof for this behavior can be given when considering the AG relation at which is shown that $r^{-3} \propto s_c(T)$ and it's reasonable to say that $\xi \sim r$ from the similar definitions, so $\xi > m \cdot s_c(T)^{-\frac{1}{3}}$ for some $m > 0$ and thus we found a lower bound for ξ that diverges as $T \rightarrow T_K$.

Tail of DOS Correlation Length There is another static lengthscale that we should briefly mention, even though we didn't calculate it in the simulations. This lengthscale is related to excess plastic modes of the supercooled system. It turns out that the two lengthscales are equivalent and that the later is accessible in lower temperatures than this PTS lengthscale.[27]

4 Other Measured Sizes

4.1 Pressure

As I'll describe in Part III, the pressure is constant and doesn't depend on the calculation itself, but there is a method to obtain the *virial pressure* in the simulation which is equal to the real applied pressure [21] and as such a good way to ensure that the simulation run as intended.

Let the system be in the canonical ensemble (*NVT*), with pair-wise additive potential $F(\mathbf{r}_{ij})$ between the particles

First we must define the *virial* as

$$\mathfrak{Vir} = \left\langle \sum_{i < j} \frac{dF}{dr}(r_{ij}) \cdot r_{ij} \right\rangle$$

where the brackets define the average value of the system (time-average\space-average is the same for ergodic systems such as liquids), for system with dimension $d = 3$ one would find that:

$$P_{vir} = \frac{NT}{V} + \frac{\mathfrak{Vir}}{dV}$$

and as mentioned above $P_{vir} = P_{applied}$.

4.2 Heat Capacity

The heat capacity C_p can be obtain via the thermodynamic definition $C_p = (\frac{\partial H}{\partial T})_{P,T}$, which in real simulation is prone to some problems, for example the fact that we only can calculate $\frac{\Delta\langle H \rangle}{\Delta T}$ in a simulation and for large ΔT the approximation $\frac{\Delta\langle H \rangle}{\Delta T} \approx (\frac{\partial H}{\partial T})_{P,T}$ might start to fail and for small ΔT noise in the measurement of $\langle H \rangle$ is critical.

One can also find C_p via the statistical thermodynamic relation:

$$\frac{\sigma_H^2}{T^2} = \frac{\langle H^2 \rangle_{NPT} - \langle H \rangle_{NPT}^2}{T^2} = C_P$$

where H is the enthalpy of the system.

Proof: the partition function in the isothermal-isobaric ensemble is $Z = \sum_i e^{-\beta(E_i + PV_i)} = \sum_i e^{-\beta H_i}$ so: $\frac{\partial Z}{\partial \beta} = -\sum_i H_i e^{-\beta H_i} = -Z \langle H \rangle_{NPT}$ and $\frac{\partial^2 Z}{\partial \beta^2} = \sum_i H_i^2 e^{-\beta H_i} = Z \langle H^2 \rangle_{NPT}$ so:

$$\begin{aligned} \langle H^2 \rangle_{NPT} - \langle H \rangle_{NPT}^2 &= \frac{1}{Z} \frac{d^2 Z}{d\beta^2} - \left(\frac{1}{Z} \frac{\partial Z}{\partial \beta} \right)^2 = \frac{\partial}{\partial \beta} \left(\frac{1}{Z} \frac{\partial Z}{\partial \beta} \right) = \frac{\partial}{\partial \beta} (-\langle H \rangle_{NPT}) = \\ &= -\frac{\partial \langle H \rangle_{NPT}}{\partial \frac{1}{T}} = -\frac{\partial T}{\partial \frac{1}{T}} \cdot \frac{\partial \langle H \rangle_{NPT}}{\partial T} = \mathbf{T}^2 \mathbf{C}_p \end{aligned}$$

Q.E.D

4.3 Entropy

The Clausius equality states that $dS = \frac{\delta Q_{rev}}{T} \stackrel{P \text{ const}}{=} \frac{dH}{T} = \frac{C_p}{T} dT$, so:

$$\Delta S = S(T_1) - S(T_2) = \int_{T_2}^{T_1} \frac{C_p}{T} dT$$

for any T_1, T_2 , so by obtaining C_p one can find the (difference in) entropy.

4.4 Free Energy

As we focus on the isobaric-isothermal ensemble, the relevant free energy is Gibbs free energy $G = H - TS$, so we can calculate $\Delta G = G(T_1) - G(T_2)$ and for single-component system $\Delta\mu = \frac{\Delta G}{n}$.

4.5 Radial Distribution Function

The *radial distribution function* defined as $g(r) = \frac{\rho(r)}{\rho_{bulk}}$ where $\rho(r)$ is the average number (or mass) density at a distance of r from a particle (i.e. on a sphere of radius r which a particle's coordinate is the center of it), ρ_{bulk} = bulk density. In $T > 0K$ $g(r \rightarrow \infty) = 1$ as particles displacement decorrelates with the distance. For a perfect crystal (with zero vibrations) $\rho(r) = \sum_i \delta(r_i - r)$ where r_i is the distance of particle i (which depends on the crystal structure) from the central particle and so $g(r)$ is a sharply peaks function. For real crystal the vibrations (and defects) broadens the peaks but the order holds well for long-range. In a liquid or glass, there is no apparent long-range order and the peaks are broader and $g(r)$ reach unity at distances of scale slightly bigger then the particle's radius. The $g(r)$ is structural dependence is useful for us to determine if the supercooled liquid solidified and also for other reasons which we'll describe later.

More “fancy” distribution functions could be:

- $g(r, \theta)$ where θ is the orientation of the central particle with respect to the displacement vector.
- $g(r, \theta_1, \theta_2)$ where θ_1 is for the central particle and θ_2 for the other particle.

both can be used in a similar fashion as the radial distribution function and sometimes are more useful as they contain more information that could be relevant to anisotropic particles.

4.5.1 Potential of Mean Force (PMF)

One uses of $g(r)$ is to obtain a simplified mean potential between particles with respect to distance. Let F be the relevant energy (H for constant P, T), so the probability density p_r to be at random uniformly distributed point in distance r from a particle at an equilibrated system obeys $\frac{p_r}{p_{bulk}} = g(r)$, but also $\frac{p_r}{p_{bulk}} = e^{-\beta F} \implies T \ln(g(r)) = F(r)$ which is the desired *potential of mean force*.

As we stated above, the “fancy” distributions can give a more general\detailed mean potential by other variables\coordination.

Part III

Computational Methods

In this part I present the computational methods used in the simulation with relevant theoretical method.

5 Simulation Methods

Some terms with brief description:

Monte Carlo Methods A class of algorithms that rely on random sampling of some space to obtain numerical results, mainly used for optimization and numerical integration. The random sampling is picking points and treating them with respect to the measure -as in measure theory- of the space. As we sample more points we get a more (statistically) accurate description of the sampled space. For example, one can calculate the energy (or any other measurable property) distribution of the system.

It is important to note that the random sampling can be obtained in different ways, as by completely random picking of points (“blind dart shooting”) or more efficient (for cases like ours) methods of random walk (as in Markov chain Monte Carlo - MCMC). For the later case, there is an assumption that we will eventually sample all (not including negligible set at most) of the states space. This assumption is connected mathematically to the definition of ergodicity for a Markov chain.

Detailed Balance and Balance Conditions The detailed balance is a sufficient condition that the given probability of a Markov chain is stationary (i.e. the equilibrium distribution of the chain holds, and if the chain is ergodic than the equilibrated state space can be sampled)[21]. The exact definition of the detailed balance needs some background and is of less importance to this project so I won’t describe it. Also, there is the balance condition which is weaker than the detailed balance but still sufficient for the statement given above, as such, it is possible for a random walk to hold one of those conditions for us to sample the equilibrated state space.

Periodic Boundary Conditions In practice, our simulations are limited to small number (ridiculously small in comparison Avogadro’s number) of particles, generally less than 10^5 . So a simulation box length l is of nanometric scale, thus almost all the particles are in the boundary of the box (boundary particles number $\propto L^2$ and general particles number $\propto L^3$) and the simulation won’t represent a real system of macro scale. A way to mimic a real system is to make the distance and displacement of particles is L -modulo for each coordinate (in the sense that particle that moves $(0, 0, L - \delta) \rightarrow (0, 0, L + \delta)$ actually moves to $(0, 0, \delta)$) and those L -periodic through each axis. This periodicity cancels the surface and all particles exhibits bulk environment, which make bulk simulations more realistic. I should note that by the minimal image convention r_c the cut-off distance of interactions between particles should be smaller than $\frac{L}{2}$, so a particle won’t feel another particle twice from different places in the periodic image.

5.1 The Metropolis-Hastings Algorithm

The Metropolis-Hastings Algorithm is a MCMC algorithm to sample the state phase of N -particles system. We’ll first write the basic algorithm in pseudo-code and then explain each line:

Metropolis Step (MS):

- Save previous Hamiltonian of the system as E_{prev} .
- Make a step that changes the state of the system and save the new Hamiltonian of the system as E_{new} .
- Pick a random $p \in [0, 1]$ of uniform distribution.
- if $e^{-\beta(E_{new} - E_{prev})} > p$: accept step (set the new system state as the current state); otherwise, reject step (return to the last state of the system).

Explanation:

- For point 4.
 - Make a “step” in the state space in a way that samples it uniformly.
 - Step can be defined as some kind of a small change of the state, the simplest step is displacing a randomly picked particle by some randomly distributed distance and changing its orientation in similar fashion. More complex step would be given as examples later in this Part.
- For next point.
- The Metropolis-Algorithm obeys the detailed balance condition and the Boltzmann distribution (the algorithm above is for the NVT condition, the extension to NPT is presented later), as the probability to move at one step from state x to state y is $p(x \rightarrow y) = \begin{cases} 1 & E_y < E_x \\ e^{-\beta(E_y - E_x)} & \text{otherwise} \end{cases}$ and $p(y \rightarrow x) = \begin{cases} 1 & E_x < E_y \\ e^{-\beta(E_x - E_y)} & \text{otherwise} \end{cases}$ so if p_x is the probability to be at state x and p_y to be at y then by detailed balance:

$$p_x \cdot p(x \rightarrow y) = p_y \cdot p(y \rightarrow x)$$

without the loss of generality, let's assume that $E_x > E_y$, then : $\frac{p_y}{p_x} = \frac{p(x \rightarrow y)}{p(y \rightarrow x)} = e^{-\beta(E_y - E_x)}$ which is with respect to the Boltzmann distribution. This result can be extended to getting from $x \rightarrow y$ via n steps by induction and thus a Markov chain which is obtained via Metropolis walk is with respect to the Boltzmann distribution.

After we defined MS, we should note that one step \neq some physical time unit, as the walk itself can be physically impossible (e.g. skips energy barriers). The previous statement is expressed even more strongly when one considers that in a large system of $N \gg 1$ one particle displacement is almost negligible, as so, we should define a more noteworthy timescale that scales with the system. We define the *MC step* as N consecutive MS's of the system, and thus the relative change (e.g. mean displacement) is independent of system scale (not including finite size artifacts) on the “timescale” of MC steps.

5.2 Advanced Monte Carlo Techniques

Monte Carlo in general is not an efficient method for getting accurate results in most cases. In the case of the molecular simulations a movement of 1 particle will include the calculation of many interactions, all for the chance that a step won't even be accepted. In the case of numerical integration it tends to converge slowly as by the central limit theorem the standard error $\sim \frac{1}{\sqrt{n}}$ with n being the number of samples.

There are some advanced extensions\methods that make the Monte Carlo simulation worthwhile (and sometimes as alternative to Molecular Dynamic simulation at which one simulate the system the N particles system where the dynamics satisfy newton laws) unlike the standard Monte Carlo simulations (as presented above,which only include steps of simple displacement),that tends to be less efficient at solving relevant problems (sampling the state space in a meaningful and fast way)[23].

Here I'll represent two of those advanced methods,I've implemented the second one in my simulations and the first one as “inspiration” for another method which I'll describe below.

5.2.1 Swap Monte Carlo

Sometimes when sampling the state space via Markov chain of simple steps (described above) there is a problem of reaching a local minima which is hard to escape,especially in the case of supercooled liquid where one might want to equilibrate the system with maximal sampling of the “supercooled space”.By clever steps sometimes the system can escape such minima essentially by ignoring relatively complex energy barriers.An example of such step is swapping spatially between 2 different (in the sense that the move would actually change the system and won't be a null move – like 2 particles with different size) randomly picked particles.Such move should occur by a constant probability (e.g. steps are displacement at probability of 0.8 and otherwise swap) to satisfy detailed balance.

In my own simulation the particles are identical but have orientation that effects the interactions,so swapping their location would give a legal swap move.A simpler to implement move which serves the same purpose is to randomly picking a new orientation to some particle (randomly chosen) instead of swapping.I've used such move and would later call it *random orienting move*.

5.2.2 Parallel Tempering

When making glasses (not in simulations) after simply cooling the supercooled liquid and exhibits glass transition, one finds the glass to be brittle and weak.The brittleness is related to the local stresses in the glass which can be released upon applied external stress of strong enough magnitude.The ultimate strength of this glass is very low (i.e. weak glass),which relates to high local structural stresses,i.e. the system is stuck in a poorly meta-stable state.A way to lower the local stress is by annealing the system,which basically means warming the system just below T_g and letting it surpass the energy barriers of the shallow local-minimas and thus reaching more stable state by slowly cooling the system down to (generally) room temperature.

A similar method could be applied to molecular simulations when trying to equilibrate a supercooled liquid,the method I'll describe now is called *Parallel Tempering (PT)* or *Replica Exchange*.[21]

In PT,one creates several simulation cells at temperatures taken from some range $\{T_1, \dots, T_k\} \subseteq [T_1, T_k]$, for simplicity we'll assume that T_i is monotonically increasing.For most of the simulation the cells runs independently of each other as in standard Monte Carlo scheme,but sometimes a move that suggest exchanging two near temperatures T_i, T_{i+1} is given.If the two temperatures are close enough so they'll have enough overlap in the state space, an actual exchange of the temperatures sometimes occur.The probability of exchanging between the two cells is given by (for NVT):

$$P(E_i, T_i \leftrightarrow E_{i+1}, T_{i+1}) = \min \left\{ 1, e^{(E_i - E_{i+1})(\beta_i - \beta_{i+1})} \right\}$$

if one suggests this move at some probability (as noted in swap moves) then detailed balance is conserved.Although simulating cells independently with exchanging them by probability is inefficient or complex to implement as it requires code with heavy monitoring on the paralleled simulations(e.g. [24]).

A simpler implementation is to pick randomly $i \in \{1, \dots, k-1\}$ and suggest the exchanging of T_i, T_{i+1} after each constant number of steps. This method doesn't hold detailed balance but regular balance - which is good enough for simulations as we noted before. Personally I've used to exchange every 10 MC steps and had 23 simulation cells.

Also, one should pick the set $\{T_1, \dots, T_k\}$ to be with good exchange rate (generally 20% acceptance for PT is considered good for efficiency), a general rule-of-thumb for T_i dependence on i is to follow logarithmic scale ($\frac{T_{i+1}}{T} = const$ for each i , which I've used). A more complex method is by estimating the overlap over the temperature range and selecting $\{T_1, \dots, T_k\}$ accordingly[25].

5.2.3 Generalization to the Isobaric-Isothermal Ensemble

The statement that we represented above were for the canonical ensemble and we would now like to briefly show the generalization of MS and PT to the isobaric-isothermal ensemble.

First, the MS is generalized by adding possible move by some probability of changing the volume of the system (and the coordinates of the particles accordingly) as $V \rightarrow V + \Delta V$ where ΔV is taken from some distribution and can be negative as the system can shrink or extend. For simplicity we would take ΔV via uniform distribution of $[-10, 10]$ with probability of 0.05 for volume change move, as we found it to be efficient enough for our simulations (volume change is more costly than regular displacement move as the interaction of all the particles must be evaluated again) and keeps the virial pressure in the vicinity of the applied pressure (up to the standard error). When one wants to keep constant pressure P , the volume change move should be accepted by the following acceptance rate (which also depends of our distribution of ΔV):

$$P(V \rightarrow V' := V + \Delta V) = \min \left\{ 1, e^{-\beta[(E(V') + PV') - (E(V) + PV)] + N \cdot \ln(\frac{V'}{V})} \right\}$$

which is essentially determined by the enthalpy with ΔV distribution-dependent fix[21].

Second, the PT is generalized by a similar fashion as the exchange probability between T_i, T_{i+1} is:

$$P(E_i, T_i, V_i \leftrightarrow E_{i+1}, T_{i+1}, V_{i+1}) = \min \left\{ 1, e^{(E_i + PV_i - (E_{i+1} + PV_{i+1}))(\beta_i - \beta_{i+1})} \right\}$$

this can be even extended to exchanging (for example) pressures and thus giving an interesting way to explore a (P, T) phase diagram[26].

6 Analysis Methods

Now I'll talk about specific computational methods that we used in the analysis.

I'll note that all measurable sizes were taken by averaging on the seemingly equilibrated part (generally the last third) of the trajectory.

Block Averaging Methods The problem with MCMC simulations is that consecutive states are highly correlated and thus we can't estimate the (thermodynamic averaged) energy of the system until we lost correlation, which demands us to do many separated simulation (PT actually makes this slightly simpler as the system losses correlation when switched, but still represents the new temperature) or to run the simulation for long enough. One might say that "the simulation ran enough time" when it sampled enough times the state phase in a meaningful way, and thus correlations have been lost many times while sampling. This idea would serve us for the next explanation of block averaging method for estimating the standard error of some measurable from the simulation.

Let our simulation trajectory be presented by $\{\text{consecutive } K \text{ somewhat correlated states}\} = B$, now we'll divide them to M blocks of equal sizes $\frac{K}{M} : B_1, \dots, B_M$. Let us define the average of an measurable A on some state set V as $\langle A \rangle_V$. Now we can define $x_i = \langle A \rangle_{B_i}$ as random variables of same distribution with mean $\mu = \lim_{|B| \rightarrow \infty} \langle A \rangle_B = \langle A \rangle$ and standard deviation $\sigma_{\frac{K}{M}}$, now we can say that $\langle A \rangle_B = \frac{\sum_{i=1}^M x_i}{M}$ with the same mean μ and s.d. should be $\sigma_{\langle A \rangle_B} \approx \frac{\sigma_{\frac{K}{M}}}{\sqrt{M}}$ if the variables $\langle A \rangle_{B_i}$ are all independent, i.e. when $\frac{K}{M}$ is large enough for losing correlation over such period, which means large enough K and small enough M . If we assume that K is large enough than as $M \rightarrow 1$ we expect that $\frac{\sigma_{\frac{K}{M}}}{\sqrt{M}} \rightarrow \text{const}$ and that this constant is the actual s.d. of $\langle A \rangle_B$ and thus the standard error.[28]

So, in practice we check if the thermodynamic quantities averages are independent of the choice of taking the last $\frac{1}{2}, \frac{1}{3}$ or $\frac{1}{4}$ of the simulation. Then by finding the maximal value of $\frac{\langle \sigma_{\frac{K}{M}} \rangle}{\sqrt{M}}$ for all $M > 4$ (I should note that the $\frac{\langle \sigma_{\frac{K}{M}} \rangle}{\sqrt{M}}$ is generally monotonically increasing with block length $\frac{K}{M}$ until it is large enough to be near $\sigma_{\langle A \rangle_B}$ as stated above) which should give us a bit of an overestimate of the standard error of A .

6.1 Implementation of PTS Correlation Length

The protocol of finding ξ' in a simulation can be found at [22] and we would describe it here.

The definition of $q(t, R), q(R), q_0$ was given at Part II. The decay of $d(R) = q(R) - q_0$ can be fitted by the next exponential form:

$$d(R) = Ae^{-(R/\xi')^u} \quad u \geq 1$$

and u suppose to increase with the decrease of T as cooperative moves of size $\sim \xi'$ or bigger in a critical way, and $u = 1$ for high temperatures.

Another generalized fit was suggested[29]:

$$d(R) = Ae^{-((R-a)/\xi')^u} \quad u \geq 1 \quad a > 0$$

with $a = 1$ by the physical motivation that a sphere with radius of 1 contain on average one particle and thus the correlation won't be strongly dependent of a growing "amorphous order" but on interaction with near neighbors, and also that for $R < 1$ the sphere have a high chance to not contain any particle and also the interactions are heavily dependent on the chosen space of the sphere and thus the non-averaged representation of $q(R)$ highly fluctuates with respect to the chosen sphere and the convergence of $d(R)$ is slow, making it less viable property for calculating/losing its significance as the mosaic state model is mean field model. It was also suggested to fix A to improve the fitting of ξ' .

The technical implementation of $q(R, t)$ would include running $q(R, t)$ 10 times on any chosen sphere and choosing 7 frames for each R and T to take the spheres from, and then average on $q(R, t \gg 1)$ to obtain $q(R)$. The actual calculation of error would be by averaging $q(R)$ for the 10 runs on the chosen sphere and then calculating the standard error for $q(R)$ by treating the 7 frame as uncorrelated. Important note that should be add up is that for a different system the standard Monte-Carlo simulation (doesn't include PT or swapping) the relations described at Part II for $q(R)$ and $\tau(R)$ don't hold, but holds when allowing swap moves[30]. Which is explained by the relaxation times dependence of energy activated movements for cavities with amorphous boundary conditions at $T < T_d$ with the note that the actual energy barriers for swap dynamics are lower than those of standard Monte-Carlo dynamics. So, as explained above, the random orientating moves serves as an alternative to the swap moves for our purpose.

Part IV

Simulation Details and Results

In this Part I'll present the details and results of the simulations for the final model. Also I'll briefly the time-consuming failed to produce glass models with intuition to why they didn't work and even were worse glass-formers than the LJ model that is briefly presented below.

Lennard-Jones Potential A widely used model for spherical particles, where the interaction has both attraction part and repulsion part. The LJ potential for interacting particles of radius σ with minimal interaction energy of ϵ as function of the distance between their centers is:

$$\psi_{LJ}^{\epsilon,\sigma}(r) = 4\epsilon \left[\left(\frac{\sigma}{r}\right)^{12} - \left(\frac{\sigma}{r}\right)^6 \right]$$

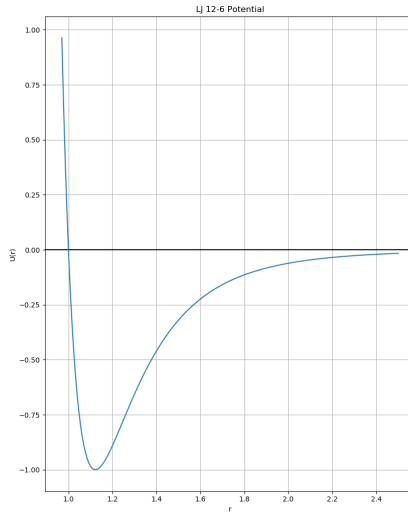


Figure 1: LJ 12-6 Potential Graph

One can see that $\psi_{LJ}^{\epsilon,\sigma}(\sigma) = 0$ and $2^{1/6}\sigma \approx 1.22\sigma$ is the minimal interaction energy distance.

We should note that ϵ has energy dimensions and σ has distance dimension, thus P, T, r, V can be represented in those units:

$$P \left[\frac{\epsilon}{\sigma^3} \right], k_B T [\epsilon^{-1}], r [\sigma], V [\sigma^3]$$

As a result, two simulations with ϵ_1, ϵ_2 and σ_1, σ_2 are equivalent if the fixed pressures and temperatures are equal when represented in ϵ_i, σ_i units. For that reason they're frequently called *reduced units*.

So for simplicity in our simulation we use $\epsilon = 1$ and $\sigma = 1$:

$$\psi_{LJ}(r) = \frac{4}{r^{12}} - \frac{4}{r^6} = \psi_{LJ}^{rep}(r) + \psi_{LJ}^{att}(r)$$

As we'll show at the simulation results, a LJ system tends to crystallize easily to an FCC/HCP structure even in the deep supercooled regions.

7 The Final Model

The final model we used is also based on the Lennard-Jones potential with some anisotropic attraction interaction which is dependent on the angles between the orientation vectors to the displacement vector.

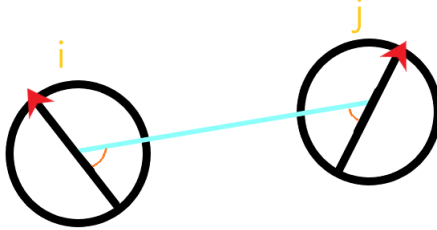


Figure 2: Illustration of 2 particles with relevant angles and distance for the interactions

In this model each particle is represented by 3D orientation (unity) vector \vec{q} and coordinates \vec{r} (Fig 2). For 2 particles i, j the displacement vector pointing from i to j is (up to periodic boundary conditions as previously described): $\vec{r}_{ij} = \vec{r}_j - \vec{r}_i = -\vec{r}_{ji}$. and the cosine of the angle θ_i between \vec{r}_{ij} to \vec{q}_i is:

$$\cos(\theta_i) = \frac{\vec{r}_{ij} \cdot \vec{q}_i}{|\vec{r}_{ij}|}, \quad \theta_i \in [0, \pi]$$

similarly for $\cos(\theta_j)$.

We define the next function:

$$u(\theta_a, \theta_b) = \begin{cases} (\cos(\theta_a) - \cos(\frac{7}{180} \cdot \pi))^2 (\cos(\frac{156}{180} \cdot \pi) - \cos(\theta_b)) (\cos(\theta_b) - \cos(\frac{170}{180} \cdot \pi)) & (\theta_a, \theta_b) \in [0, \frac{7}{180} \cdot \pi] \times [\frac{156}{180} \cdot \pi, \frac{170}{180} \cdot \pi] \\ 0 & otherwise \end{cases}$$

which obtains a maximal value at $\theta_a = 0$ and $\theta_b \approx \frac{161.7}{180} \cdot \pi$, these angles are such that the anisotropic interaction make the FCC/HCP structures unfavorable to some extent.

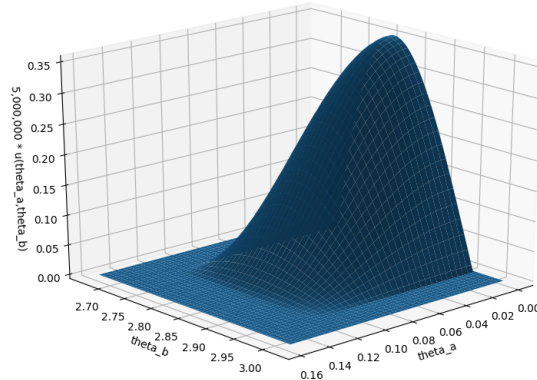


Figure 3: Graph of $5 \cdot 10^6 \cdot u(\theta_a, \theta_b)$ in and near the support of u

Now we can finally define the interaction potential between i and j :

$$\psi_M(\theta_i, \theta_j, r) = 4 \left[\frac{1}{r^{12}} - \frac{1}{r^6} \cdot (1 + C(u(\theta_i, \theta_j) + u(\theta_j, \theta_i))) \right] = \psi_{LJ}^{rep}(r) + \psi_{LJ}^{att}(r) + C \cdot \psi_{aniso}^{att}(\theta_i, \theta_j, r)$$

with C serves as anisotropic interaction strength factor (or Orientational factor).

The fact that $u(\theta_a, \theta_b) \neq 0 \implies u(\theta_b, \theta_a) = 0$ is trivial and means that the interaction won't be count twice. The orientation that maximize ψ_{aniso}^{att} (for any distance r) between 3 particles is illustrated below, and it can be seen that a particle can have only two relatively "strong bonds" – by the definition of bond that is given below. As a result of such ordering, one can expect to obtain some chain structures in the simulations, which we'll show that is correct to some extent for sufficiently large C . As explained in Part II, such interaction would make the supercooled system favor network forming and thus the glass is less fragile with the increase of C .

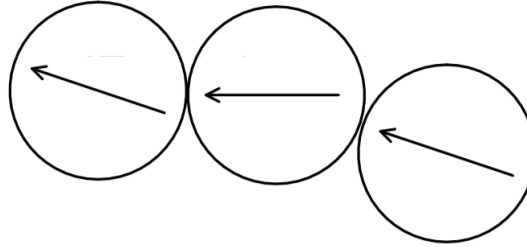


Figure 4: Favored ordering for 3 particles

It should be noted that the above order doesn't fit with the FCC/HCP packing

One final note is that the value of C for non-negligible ψ_{aniso}^{att} is in the order of $\sim 10^7$ or more which is seemingly large. This relates to the Taylor expansion of cosine in 0 and π , which roughly gives $u(\theta_a, \theta_b) \sim [(\theta_a)(\pi - \theta_b)]^4$ which is a very small number if $(\theta_a, \theta_b) \in [0, \frac{7}{180} \cdot \pi] \times [\frac{156}{180} \cdot \pi, \frac{170}{180} \cdot \pi]$.

The minima for ψ_M is in $r_{min} \approx \left(\frac{2}{1+7.05 \cdot 10^{-8} \cdot C} \right)^{1/6}$ thus for $C < 7 \cdot 10^7$ the shift from the LJ r_{min} is less than 0.01 and pretty negligible. Also, ψ_M vanishes at $1 > r_0 > \left(\frac{1}{1+7.05 \cdot 10^{-8} \cdot C} \right)^{1/6}$ and for $C < 3 \cdot 10^7$: $r_0 \geq 0.83$ this value differs from the LJ r_0 and could also effect the nature of the system.

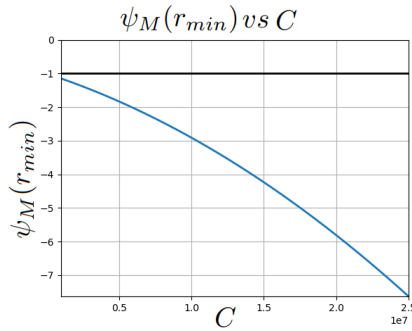


Figure 5: Graph of $\psi_M(r_{min})$ * dependence of C

*At optimal orientations

The black bold line $y = -1$ represent the ψ_{LJ} minima. A way to look at the graph above is how much a "bond" in the optimal orientation, for example: if $\psi_M(r_{min}) = -5$ than such "bond" has the energy equivalent to a total of 5 LJ near interactions.

8 Failed Trials and Conclusions

After we introduced the final model we can discuss the previous poorly glass former models and show they're tendency to crystallize (more than the LJ liquid!).

All of the models are similar to the final model as they have orientation vectors and orientation dependent interactions. The main nuance of the final model is that the orientation interaction are relative to the displacement vector unlike the previous models where the relative only to each other orientation,independent of displacement. This independence on the displacement vector orientation relative to the orientation of the particles means that the interaction is isotropic (for 2 particles with fixed orientation vectors) and the relative orientation dependence "masks" this fact – soon we'll show that this isotropy helps the liquid to crystallize. I'll now represent one of those models(as they behave similarly because the),some results of crystallization for this model and the favored ordering in the crystalline structure.

Lets take the final model particles and define them different ψ_{aniso} ,although when we would call it now ψ_{iso} by the last argument.First we most define $\theta_{ij} \in [0, \pi]$ as the angle between \vec{q}_i, \vec{q}_j , so:

$$\cos(\theta_{ij}) = \vec{q}_i \cdot \vec{q}_j \implies \sin^2(\theta_{ij}) = (1 - (\vec{q}_i \cdot \vec{q}_j)^2)$$

Now we finally can define $\psi_{iso}(r, \theta)$:

$$\psi_{iso}(r, \theta) = \frac{\sin^{12}(\theta)}{r^6}$$

We'll call this model the Sine12 model.

For this model particles favor ordering with orthogonal orientation relative to their neighbor's orientation,because $\sin^{12}(\frac{\pi}{2}) = 1$.Also the orientation vector and its negative (like $-\hat{x}$ and \hat{x}) interacts equivalently.

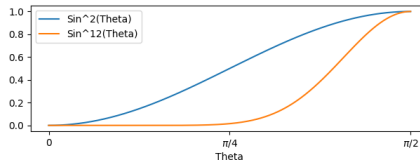


Figure 6: Graph of $\sin^2(\theta)$ and $\sin^{12}(\theta)$

For illustrating at which angle the interaction is favorable and that $\sin^n(\theta)$ becomes more sharp with the increase of n ,meaning that the orientations should be nearly orthogonal for a significant orientational interaction.

A difference between the range in which C make $C \cdot \psi_{aniso/iso}$ non-negligible.For ψ_{iso} even $C > 0.1$ gives a relatively strong interaction as $\sin^{12}(\frac{\pi}{2}) = 1$ unlike ψ_{aniso} for which the order of magnitude is $C \sim 10^7$.

We ran standard Monte-Carlo simulations (without PT or swap) with the same scheme for $C = 0.9$ and $C = 0$ (i.e. LJ potential) for several temperatures in $[0.6, 1.7]$ with $P = 1.14$ for all the simulations ,number of particles is $N_{Sine12} = 300, N_{LJ} = 400$.All the systems where cooled down from $T_0 = 1.8$ to their assigned temperature at a rate of $\frac{0.000033}{MC Step}$ and then sampled every 200 MC Steps and ran for 100,000 MC Steps.

The main point can be seen by comparing the V, T diagrams (described below):

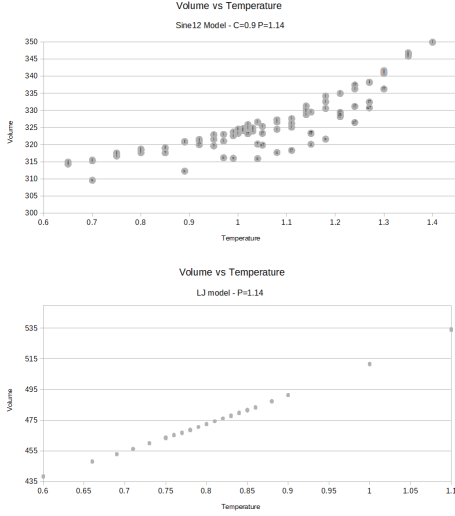


Figure 7: V,T diagrams for $C = 0$ -LJ- (below) and $C = 0.9$ (above) under the simulation scheme given above

It should be noted that some of the simulations didn't converge (labeled as '?') and some points were assigned a phase ('s'-solid,'l'-liquid) which was determined by the peaks of the $g(r)$ as explained in Part II and the decrease in volume that occurs in the liquid-solid transition. For the LJ the assignment of phases was unnecessary as none of them crystallized-also, the average volume for each run of the LJ model falls on each other, which indicate that the system indeed reach equilibrium.

So, by the same simulation protocol for the 2 systems, the 3 runs of the LJ thermodynamic variables (specifically V in the graph above) falls on each other – so we can conclude that the LJ system reach (thermodynamic or meta-stable) equilibrium, unlike the Sine12 system that sometimes crystallized or began crystallization near the end of the run.

The conclusion from the above is that T_m of the Sine12 system is higher than T_m of the LJ system (≈ 0.8 [31]), which indicate more enthalpy gain by the freezing of the Sine12 system. Also, the fact that the LJ system didn't freeze shows that the stability of supercooled LJ fluid is better than that of the supercooled Sine12 fluid. All of the above can be explained easily when one sees that there is an energy favorable (at-least in the near neighbors level) “orientational structure” for the close-packing structure where each particles is orthogonal to 10 out of its 12 neighbors:

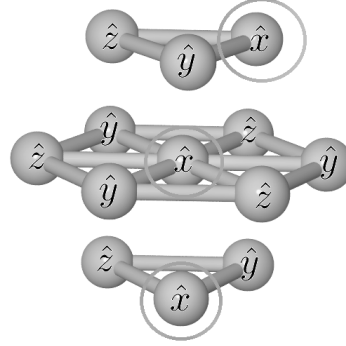


Figure 8: Energy favored orientation of nearest neighbors for close-packing structure of the Sin12 model

The orientations that presented above are of $\hat{x}, \hat{y}, \hat{z}$ which is an orthonormal basis of \mathbb{R}^3 . The circled particles are those with the same orientation (zero orientational interaction)

In the simulations it seems that the average number of orthogonal neighbors in the crystal structure of the Sine12 model is about 9, which resembles the value suggested above. But as this model was abandoned I really didn't investigate it too much.

9 Simulation Details - The Final Model

Note: The simulations and analysis were written fully from scratch in Python 3 , thus had poor efficiency which limited the number of particles and steps for reasonable run time.

For each $C \in \{0, 0.7 \cdot 10^7, 1.0 \cdot 10^7, 1.3 \cdot 10^7, 1.5 \cdot 10^7, 1.6 \cdot 10^7, 1.7 \cdot 10^7, 1.8 \cdot 10^7, 2.0 \cdot 10^7\}$ we ran Monte-Carlo PT Simulations with 23 different cells with $N = 400$ particles each at a temperature from the range of $\{0.2, 0.36\}$ with selection of temperatures by a geometric series with $a_1 = 0.2, a_{23} = 0.36$ (the logarithmic scaling rule-of-thumb described in Part III) under the isobaric-isothermal ensemble with $P = 0.01$. It should be noted that the potential was truncated and shifted at $r_c = 3.0$. Before using parallel tempering all the systems were cooled down from $T_0 = 0.8$ to their assigned temperature at a rate of $\frac{0.0000033}{MC Step}$ (about 18,000 MC Steps per cell) to avoid crystallization that occurs at $T \approx 0.53$ for the LJ case[26](and as we'll see, even under this temperature). The PT we use is the simple version detailed at Part III that holds the balance condition at the protocol explained there. The possible moves at each MS were:

1. Displacement of coordinate (by distance of 0.04 selected from Gaussian distribution with s.d. of 0.3·0.04)
– $p = 0.95$
 - (a) and orientation (change of 0.005 rads from previous orientation) – $p = 0.95^1$
 - (b) and randomly selected orientation – $p = 0.05$
2. Change volume by random $\Delta V \in [-10, 10]$ uniformly distributed – $p = 0.05$

A frame was saved to the trajectory once every 300 MC Steps.

The actual number of steps for each simulation is described in the next section.

¹both the displacement distance and change of orientation were determined so for all simulations the acceptance rate would be above 0.2

10 Results and Discussion

Most simulations ran for about 350,000 MC Steps, some have seem to equilibrate (i.e. thermodynamic quantities didn't change with time), mainly the higher temperatures\weaker orientational interactions as one might expect.

The main reason for not reaching equilibrium is the (relatively) short run of the simulation, due to technical issues. To be exact, the servers are set to run each simulation for a max of 2 weeks, a fact I didn't know and because of technical difficulties I didn't continued the run afterward, at least not at the time scope of the Amirim project. So the analysis is more for showing some qualitative results than of a finished project, and should be treated as such.

We found the results to be interesting for $C \in \{0(\text{LJ}), 1.3 \cdot 10^7, 1.5 \cdot 10^7, 1.6 \cdot 10^7, 1.7 \cdot 10^7, 2.0 \cdot 10^7\}$ (unfortunately the simulation of $1.8 \cdot 10^7$ ran on a slower processor thus reached only 145,000 MC Steps and failed to equilibrate), as crystallization wasn't observed for $C \geq 1.5 \cdot 10^7$, unlike the LJ case where all the boxes crystallized or the case of $1.3 \cdot 10^7$ where crystallization was rare – occurred only in 1 box. All of this is explained by the graphs, tables and discussion below.

10.0.1 Standard Thermodynamic Sizes

We'll now show graphically the temperature dependence of several measurables:

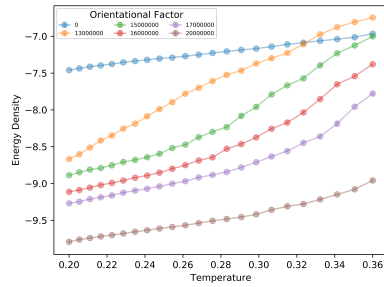


Figure 9: Energy Density ($\frac{E}{N}$) vs Temperature for the different runs

As we can see the energy for the LJ system is almost linear and doesn't indicate any first order phase change. As we'll see by the radial distribution function all the LJ boxes actually crystallized and equilibrated. All the other curves (except for $C = 1.3 \cdot 10^7$) are convex, as expected by the occurrence glass transition or slowing down of the dynamics. As we stated above, the lower temperatures didn't reach their equilibrium energy and were in higher energy (for example: figure below), a fact that can be related to the slowing down, as this phenomena is observed in the lower temperature region and for higher C values.

For $C = 1.3 \cdot 10^7$ we obtained different behavior that can be explained by that the supercooled liquid is unstable, because some of the boxes crystallized (next sub-section).

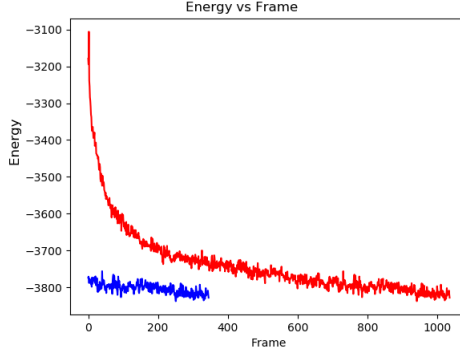


Figure 10: Energy vs Frame (300 MC Steps) for $T = 0.275593863982$ and $C = 2.0 \cdot 10^7$

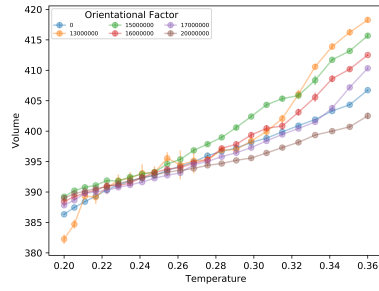


Figure 11: Volume vs Temperature for the different runs

There is a general trend (for $C \geq 1.5 \cdot 10^7$ and the higher range of temperatures) of small decreasing in volume with the increase of the orientational factor. We can relate this trend to the decrease of r_0 and the increasing tendency of particles to be “bonded” (will be explained later) to each other at the r_{min} distance as a result of the deep energy well, we claim that the second argument is of more importance as by the radial distribution functions that shows a large peak (with max > 10) near r_{min} .

For the lower temperatures ($C \geq 1.5 \cdot 10^7$) it seems that the volumes are almost independent of C . I claim that this fact relates to the similar semi-amorphous structure of the weakly networked systems which is independent of C for low enough temperatures, more in the next sub-section.

For $C = 1.3 \cdot 10^7$ and $C = 0$ some of the boxes crystallized and therefore are more dense than the supercooled phase and as a result those two don’t follow the trend.

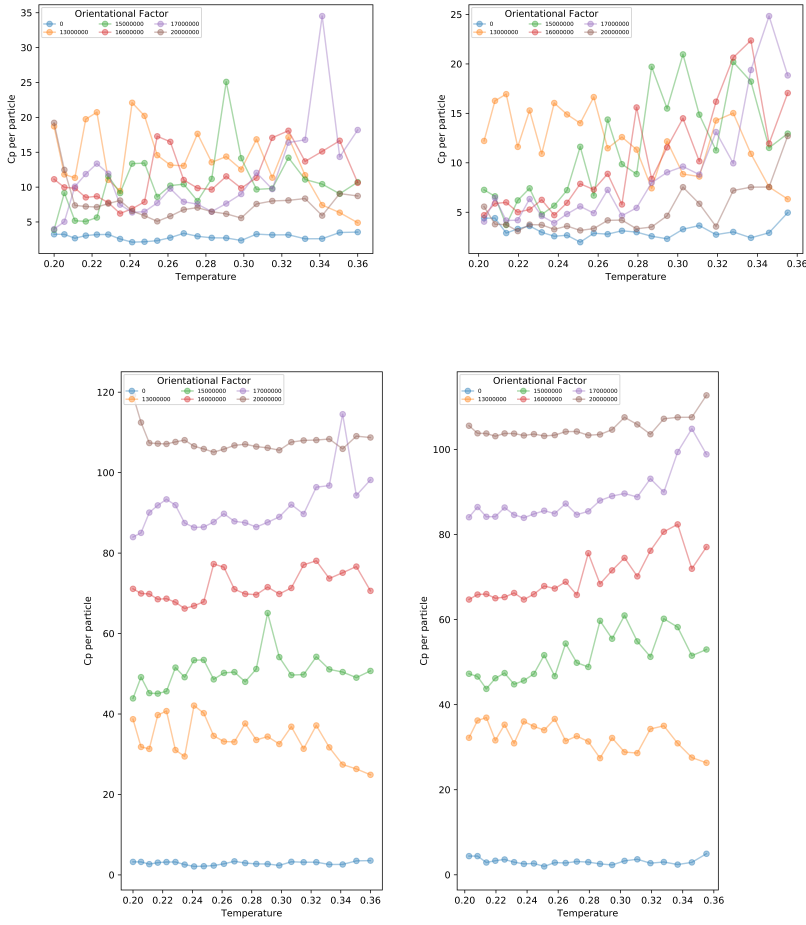


Figure 12: Heat Capacity per particle ($\frac{C_p}{N}$) vs Temperature for the different runs: by enthalpy variance (left) and $\frac{\Delta H}{\Delta T}$ (right) and same graphs with each curve shifted by 20 for clearance (below)

The heat capacities obtained by both methods (especially from Energy fluctuations) fluctuates significantly with the temperature, indicating that the values didn't converge yet and that longer simulation times are necessary. Thus we can't conclude the behavior of the heat capacity with high certainty. But I think that for $C \geq 1.5 \cdot 10^7$ there is maybe a trend of increasing heat capacity with temperature, a description that would fit well with the behavior of C_p in the vicinity of the glass transition.

For $C = 2.0 \cdot 10^7$ this suggested trend is more pronounced in the values extracted from $\frac{\Delta H}{\Delta T}$. It should be noted that the heat capacity which is extracted via energy fluctuations would generally be higher than the actual heat capacity for systems that on the way to reach equilibrium (and thermodynamically irrelevant as the system is not stable), as the energy tend to vary more when the system is unstable (example: Fig.12). For $C = 1.3 \cdot 10^7$ the system is highly unstable in lower temperatures as crystallization occurs and therefore doesn't follow the suggested trend. For the LJ system the heat capacity is more stable, indicating that its value converged and that the system reached equilibrium for all\most temperatures.

Also, It seems that the fluctuations of the heat capacity increases with the temperature and decreases with the orientational factor. This can be related to the slow down in dynamic and loss in degrees of freedom as "bonds" are created.

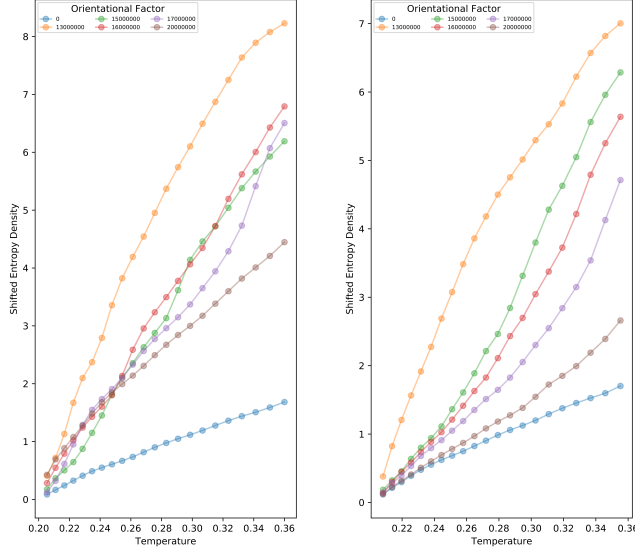


Figure 13: Entropy Density ($\frac{S}{N}$) shifted by $-S(T = 0.2)$ vs Temperature for the different runs, by C_p from enthalpy variance (left) and $\frac{\Delta H}{\Delta T}$ (right)

The entropy (relative to the entropy in $T = 0.2$) is calculated from the heat capacity and thus its accuracy is bad as it derived from the inexact heat capacities. I don't think that the results are accurate enough to give any meaningful conclusion.

10.0.2 Radial distribution Functions and Structure

Now we'll present and discuss about the $g(r)$ of the different systems.

First of all, the LJ systems crystallized as can be seen by the $g(r)$ (Fig below), although for the higher temperatures the peaks of the $g(r)$ broadens and some even vanishes because of vibrations.

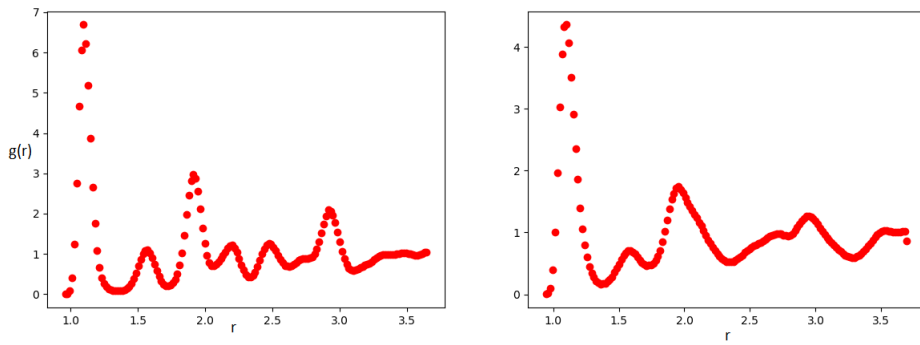


Figure 14: Radial distribution function for simulated LJ system at $T = 0.235$ (left) and $T = 0.36$ (right)

for all $C \leq 1.3 \cdot 10^7$ a similar $g(r)$ was observed, with the exception that the first peak of $g(r)$ is extremely

high for the simulations where most particles were bonded (bond defined below) as particles who are bonded generally stick close to the depth of the energy well. As such, this effect is observed for all $C \geq 1.3 \cdot 10^7$ so I'll show the $g(r)$ without the first peak (i.e. $r \geq 1.3$) – as it would be less beneficial for understanding the structure.

The $g(r)$ ($r \geq 1.3$) for $C \geq 1.5 \cdot 10^7$ for most simulations is as expected from liquid (Fig below) which indicates that the systems not crystallized.

For the lower temperature range a small peak (over another peak) is observed at $r \approx 2.0$ which can be related to particles with 2 bonds (if $A - B$ and $B - C$ are bonded then the distance of A and C is a bit less than 2.0)

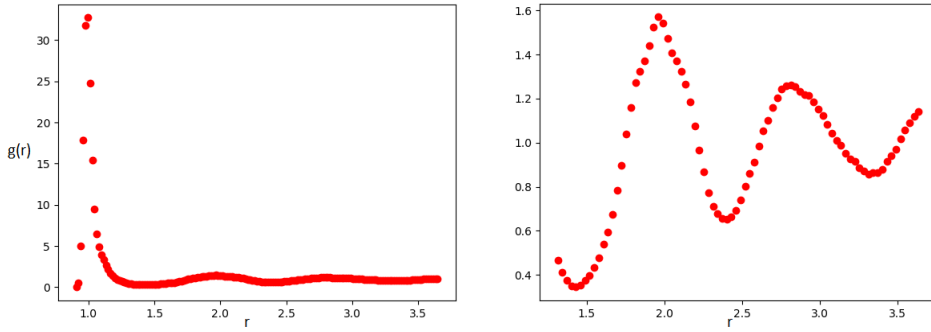


Figure 15: Radial distribution function for simulated $C = 1.5 \cdot 10^7$ system at $T = 0.235$, with the first peak included (upper left) and without it (upper right)

When visually inspecting the low temperature simulations one can see some short range layering of particles:

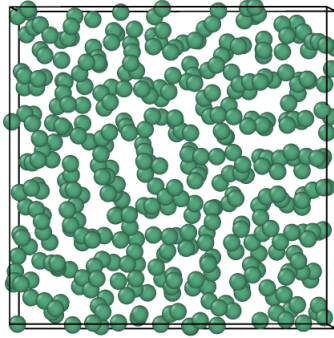


Figure 16: A selected frame of system with $C = 1.7 \cdot 10^7$ and $T = 0.2$ which clearly shows some layering and short ordering

This suggests that some short range ordering occurs at the lower temperature range. The short range of the phenomena might be an artifact as a result of small system size and thus I believe that the run and analysis of bigger simulation is necessary.

From the $g(r)$ we can find the Potential of Mean Force (*PMF*), example for $T = 0.235, C = 1.5 \cdot 10^7$:

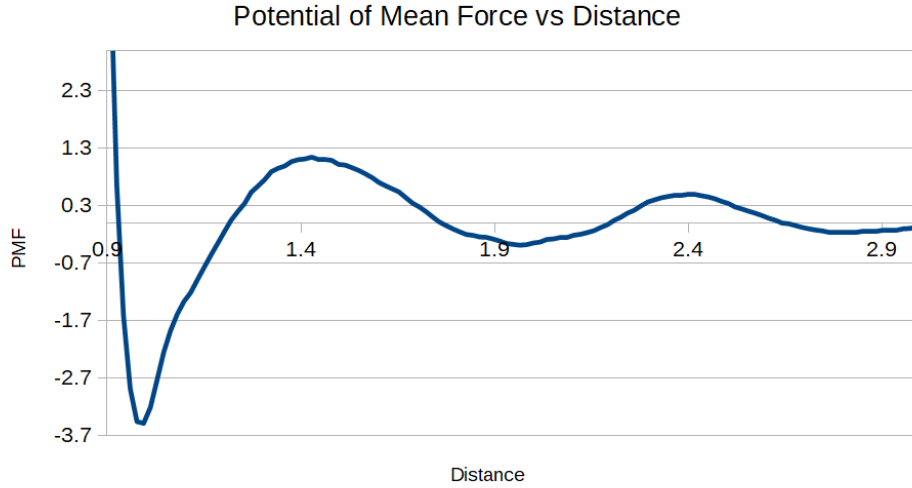


Figure 17: Potential of Mean Force as a function of distance for $T = 0.235$ and $C = 1.5 \cdot 10^7$

As the potential of mean force represent the effective free energy at some distance at the units of kT , we can conclude that the first neighbors interaction is about $3 - 4 kT$ which means that the movement of nearest neighbors is very unlikely at the given range of temperatures. Which can result in the vanish of energy activated relaxation processes, including the ones that lead to crystallization. We should note that this simple PMF is far from perfect to describe the actual highly orientation-based interaction in our systems.

To overcome this problem we'll obtain the PMF (and the radial distribution function) as a function of r, θ – where r is the distance between particles and θ is the angle (in radians) between the particle's orientation vector and the displacement vector.

We've extracted the $PMF(r, \theta), g(r, \theta)$ for a selected systems with $C \geq 1.5 \cdot 10^7$: (avoiding θ with $\sin(\theta) < 0.122$ as the normalization factor for such angles in the $g(r, \theta)$ is big, meaning that this angle is not probable – except $\theta \sim 5^\circ$ in which ψ_{aniso} is favorable)

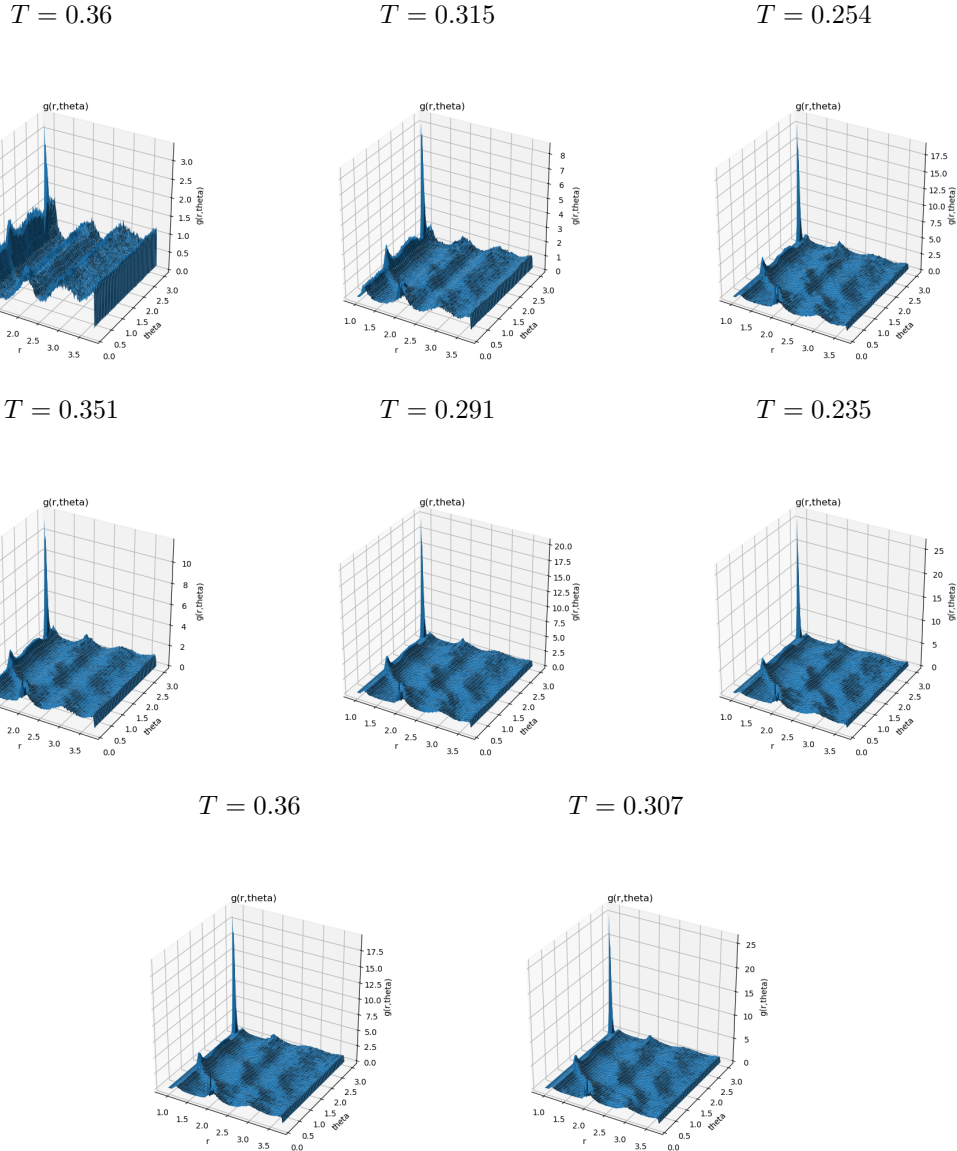


Figure 18: $g(r, \theta)$ for $C = 1.5 \cdot 10^7$ (up), $C = 1.7 \cdot 10^7$ (middle), $C = 2.0 \cdot 10^7$ (down) at different Temperatures.

In the $g(r, \theta)$ graph it is apparent that the structure becomes more anisotropic (as expected by network forming particles) with the increase of C and decrease of T . Also, because \log is monotonically increasing this trend is also observed in the $PMF(r, \theta)$ graphs below. The most noticeable anisotropic behavior is the bow shaped hill from $(\theta \approx 1.1, r \approx 1.0)$ to $(\theta \approx 0.1, r \approx 1.2)$ where another peak forms (probably related to the next neighbor on a 3 particles chain—which is at distance $r \approx 2$ with small θ). Another shallower hills with similar shapes are observed at higher r, θ . Both of this are directly related to the suggested increase in order and layering. The origin of this behavior couldn't simply be linked to ψ_{aniso} behavior as for $\theta \in (0.13, 1.1)$ $\psi_{aniso} \equiv 0$, so we can conclude that it relates to a meta-stable favored ordering. We should note that this behavior makes the part of the first layer of neighbors somewhat further than the LJ liquid case and probably is related to the fact that at the lower temperature region the volumes of all the systems with $C \geq 1.5 \cdot 10^7$ are almost equal. I'll note that the highest peak in $r \approx 0.95, \theta \approx 163^\circ$ seems not only to increase in height

but also becomes more sharp with the anisotropy. For $C = 2.0 \cdot 10^7$ no major structural change is observed via $g(r, \theta)$.

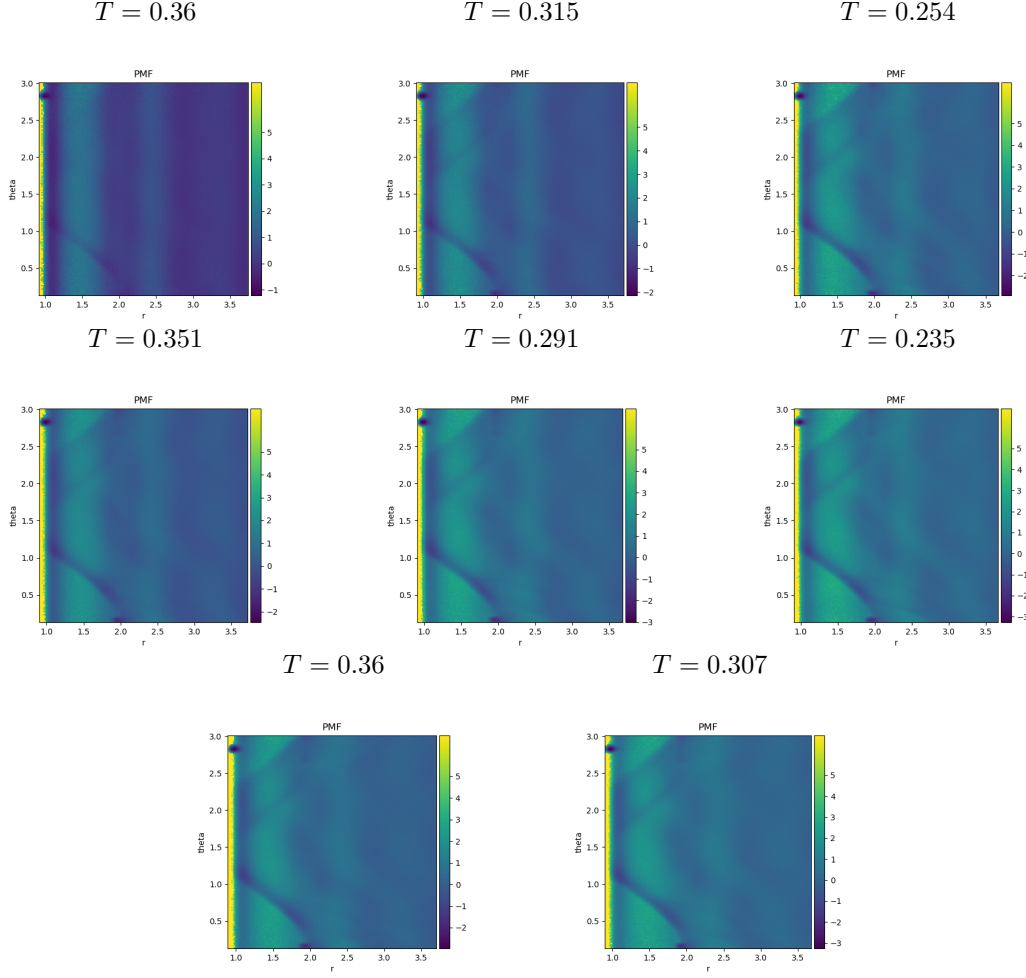


Figure 19: $PMF(r, \theta)$ for $C = 1.5 \cdot 10^7$ (up), $C = 1.7 \cdot 10^7$ (middle), $C = 2.0 \cdot 10^7$ (down) at different Temperatures.

The $PMF(r, \theta)$ give us the information of $PMF(r)$ from above with angular dependence. We can see that the main contribution to the first peak of $PMF(r)$ is of $\theta \approx 163^\circ$ (and correspondingly the not shown $\theta \approx 0$) as expected and with the value of $2 \sim 3kT$ (depends on temperature in fairly trivial manner) and for $C = 1.5 \cdot 10^7$ this peak seems to sharpen with the decrease of temperature – a similar behavior is expected for all the cases, though this check would be accessible with the increase in resolution of the $g(r, \theta)$ (which should be done on a larger set of samples). The second peak and bows are also become more of an energy wells in the expected trend – and become deeper then $1kT$ for low enough temperature which is increasing with C as we can deduce by the trend, through not directly calculated.

When the energy barrier of escaping the “bow” grows larger relatively to $1kT$ the systems short range ordering should and does significantly increase.

Extracting g and PMF for the variables r, θ_1, θ_2 (θ_1 and θ_2 were described in the introduction of the potential) would give us the full image of the system and would be beneficial for the extraction of thermodynamic sizes, but this extraction is outside the scope of this work due to limitations of time and the number of samples

needed to estimate this functions up to good accuracy (in comparison the $g(r, \theta)$ seems already noisy for our current samples set).

Bond Definition We define a “bond” as 2 particles whose distance is $r \leq 1.3$ and $\frac{\psi_{aniso}(r, \theta_1, \theta_2)}{\psi_{aniso}^{max}(r)} > 0.2$, i.e. the particles are close enough to be nearest neighbors and the interaction is somewhat significant with respect to its minimal (through maximal in absolute value) value.

Now that we’ve defined bonds we can count the particles that are in a bond and those that have 2 bonds.

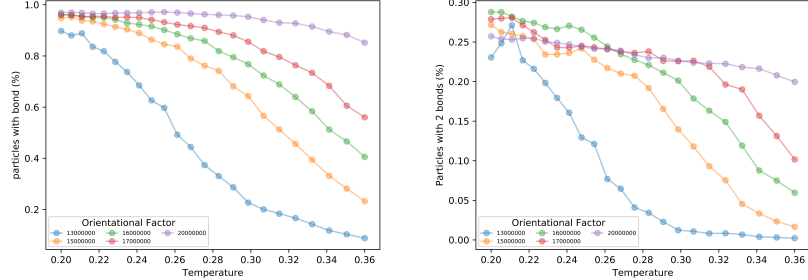


Figure 20: percentage of particles in a bond (left) / 2 bonds (right) vs Temperature for the different runs

As we can see, the saturation of the first bond increases with the decrease in temperature and for the lower temperatures almost all of the particles are in a bond, which is reasonable as enthalpy dominates Gibbs free energy in those regions. For a given temperature, the number of bonded particles increase with C , which is in agreement with the enthalpy argument. The dependence of percentage of two bonded particles of temperature is similar. For $C = 2.0 \cdot 10^7$ the saturation of bonding is almost 1.0, which fits with the structural consistency of it for the given temperature range.

An interesting remark is that for the lower temperatures all the curves are relatively close to each other in both graphs. This similarity hints a similar amorphous structure for all systems with $C \geq 1.5 \cdot 10^7$ in the supercooled region. This conclusion of similar structure can be stretched to higher temperatures by examining the relatively low dependence of $\frac{\text{probability to be with 2 bonds}}{(\text{probability to be bonded})^2}$ in T and C^2 . We should note that the fact that $\frac{\text{probability to be with 2 bonds}}{(\text{probability to be bonded})^2} \approx 0.3 < 1$ shows that the second bond is cooperatively unfavorable – at least in the sense that if one bonding site is bonded then it is less likely for the other to be bonded as well.

Most remarkably, the solid phase of $C = 1.3 \cdot 10^7$ manages to keep a high percentage of bonded particles (more than the supercooled phase in the higher temperatures) – which is not surprising as explained in the introduction of the final model, the existence on single bond is in agreement with the close-packing structures – and has almost the same percentage of 2 bonded particles as the supercooled phase – this is more surprising as the pure FCC structure is not compatible with 2 bonds on the same particle. The conclusion by this fact is that our model has a very stable close-packed solid state, which is only hindered by the relatively high energy barriers introduced by ψ_{aniso} at a low T .

²I’ll note that $\frac{\text{probability to be with 2 bonds}}{(\text{probability to be bonded})^2}$ has higher dependence in T and C

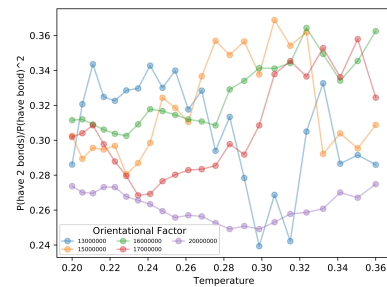


Figure 21: $\frac{\text{probability to be with 2 bonds}}{(\text{probability to be bonded})^2}$ vs Temperature for the different runs

PTS Lengthscale The protocol of extracting ξ' is described at Part III. And the results are (for $q(R) - q(2.9)$):

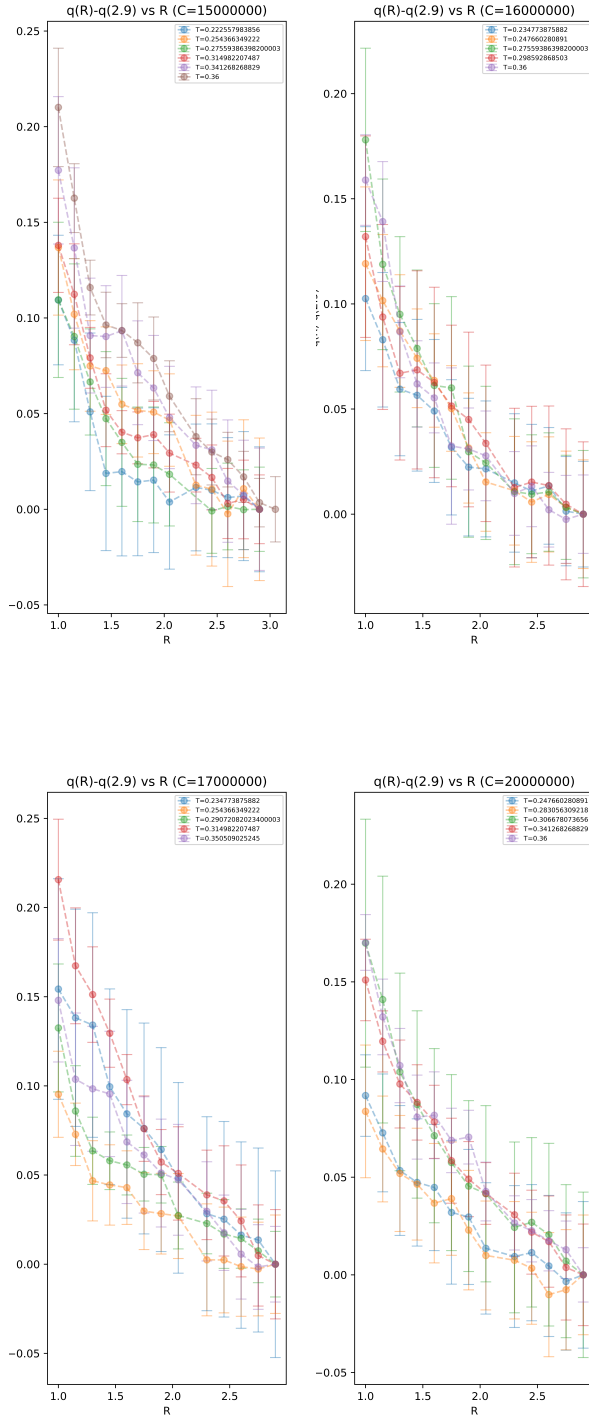


Figure 22: $q(R) - q(2.9)$ for several temperature for each $C \in \{1.5 \cdot 10^7, 1.6 \cdot 10^7, 1.7 \cdot 10^7, 2.0 \cdot 10^7\}$

The results of $q(R)$ for $R \leq 2.9$ (the maximal radius we obtained results of before the deadline of this project) shows that q is monotonically decreasing with R as expected, though the decrease is inconsistent (seems almost constant on some ranges for some of the systems – which is very reasonable for networked systems) and $q(R)$ doesn't follow an exact trend when comparing different temperatures and orientational factors. For the higher range of R_s we'll expect the $q(R)$ would get closer to q_∞ , if we'll assume that $q(2.9)$ is relatively close to q_∞ then q_∞ doesn't show the expected trend of decreasing with T as more states are accessible at higher temperatures – on the other hand, the fact that this trend isn't observed might indicate that $R = 2.9$ is still too small for estimating q_∞ .

This results can be explained in 2 ways: 1) for small R_s (especially $R < 2$) it should be expected that Γ (the entropic loss per area unit due to mismatch) is highly dependent on the selected cavity and its radius meaning that the mean-field assumptions on the boundary doesn't work – this is not surprising as our particles has some tendency to create networks due to their low network-forming. This fact is also expressed in the higher variance (and standard error) of the measure $q(R)$ for relatively small R . 2) it seems that the error of $q(R)$ is most of the times bigger than level of $q(R) - q(R+0.15)$, this error is also the error of $q(R) - q_\infty$ which might give us a highly inaccurate description of this quantity and also explain the absence of any trend.

Both problems can be somewhat solved by increasing the number of tested unrelated cavities or by a more biased method where the measured systems have the same hysteresis (e.g. using the same box after equilibration at $T = 0.36$ and than equilibrate the same box over different C_s and T_s and measure from it the value of $q(R) - q_\infty$). I should also note that a simulation with more particles will let us measure $q(R)$ for bigger R_s ($R < \frac{L}{2}$ for the minimal image convention) which might be necessary for estimating q_∞ .

All the above and some personal tries leads to the conclusion that the fitting of the results at the form of decreasing exponential won't give us the true value of ξ' . When I was trying to fit the data the fitted parameters were highly dependent on the method of picking (for example, I tried applying a constant pre-exponential factor for getting a better fit and for slightly different values of it I got high difference in ξ' values) and don't follow an apparent trend.

There is also a possibility that this extraction of ξ' as exponential decay might be a bad description (or just that our measure would slowly converge) for our system and other parameters that fit such system would be better.

Part V

Summary

In this project the effects of the addition of a simple anisotropic interaction to a single-component LJ system were explored. The strength of the interactions was determined by a factor C . The anisotropic interactions were found to hinder the crystallization of the system with the increase of C and thus served as a source of frustration to the system. Though it should be noted that the FCC phase was stable and probably represent the exact (up to some defects to exploit the anisotropic interactions) solution to the stable solid phase of the system.

Some of the systems on which the results were based didn't reach meta-stability thus shouldn't be treated as an accurate description of the system but only in a semi-qualitative way.

A way we tried to measure a possible glass transition was with the ξ' , which didn't seem to show the expected behavior for a fragile glass – even at the lower range of C s, which might indicate that our system doesn't behave as a supercooled liquid reach T_g as a fragile glass, though the convergence rate of the quantity that let us obtain ξ' seems too slow, atleast at the scales of our system of few hundred particles.

Another thing that we've noticed is the increasing short range order and layering of the anisotropic systems along with the increasing in bonded particles percentage – indicating a structural change with the fall of the system to some specific meta-stable states that is more related to the geometry of the potential than the strength when C is large enough.

Few things need to be done so we'll be able to treat the results with quantitative respect: increasing the size of the systems, longer running time of equilibration, sampling of much more states for the extraction of ξ' (if even possible), using different tools to analyze the possible glass transition of this somewhat network forming system.

I can summarize by saying that personally the work opened this subject to me and its has a potential to explore the behavior of systems with low network forming tendency.

Fin



Part VI

Appendices

11 Appendix A: Ising Model Simulations and Results

The Ising model is a simplified model for particles with magnetic spin. In its simplest form the interaction is with nearest neighbors and the particles are placed on a lattice.

In such lattice, particle i with spin $s_i = \pm 1$ would have k neighbors (depends on the dimensions of the system and the lattice structure), we'll symbol the j^{th} neighbor by n_j . The energy of particle i is defined as:

$$U_i = \frac{1}{2} \sum_{j=1}^k J_{in_j} s_i \cdot s_{n_j}$$

J_{in_j} is an interaction constant between the 2 particles. It is not necessary that J_{in_j} would be all equal (as in the case of spin-glass, where randomly picked J_{in_j} tend to add frustration to the system) but in the simplest case can be all set to be +1 (ferromagnetic) or -1 (anti-ferromagnetic).

For the ferromagnetic case for 2D hexagonal (or cubic) lattice it is known that with the decrease of T a 2nd order transition occurs (at Curie temperature, which is analogous to the real world Curie temperature of metals) with the magnetization $M = \frac{\sum_{i=1}^N s_i}{N}$ as an order parameter. For the anti-ferromagnetic case, the magnetization is 0 for every T and therefore can't be used as an order parameter that relates to any 2nd order transition.

I ran some standard Monte Carlo simulations of hexagonal 2D lattice with anti-ferromagnetic ($J = -5$) and cubic lattice ferromagnetic ($J = 5$) interactions (Fig.23), and it can be seen that the magnetization doesn't grow by a power law with the decrease of T , and the structure seems to be disordered but with a trend that most particles have 2 neighbors with the same spin and 4 with opposite spin (Fig.24).

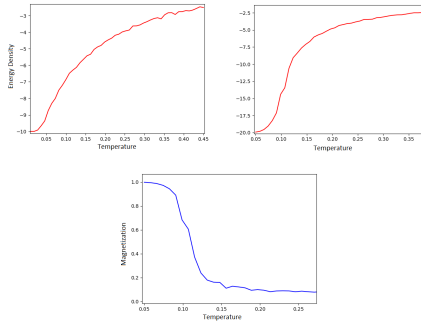


Figure 23: Energy Vs Temperature for hexagonal anti-ferro case (upper-left) and cubic ferro case (upper-right), Magnetization vs Temperature for the cubic ferro case (lower)

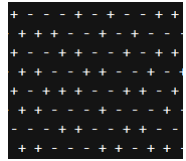


Figure 24: Typical state of the 2D hexagonal anti-ferro Ising model

$+$ = spin up , $-$ = spin down

Part VII

References

References

- [1] J. D. van der Waals, Ph.D. thesis, Univ. Leiden (1873), english translation: Phys. Mem., vol. 1, p. 333, 1890.
- [2] W. Kauzmann, Chem. Rev. 43, 219 (1948).
- [3] L.-M. Martinez and C. A. Angell, Nature 410, 663 (2001).
- [4] Debenedetti, P. G. (1996). Metastable liquids: Concepts and principles. Princeton, N.J: Princeton University Press.
- [5] Grigera T. S. and Parisi G., Phys. Rev. E, 63 (2001) 045102(R).
- [6] Blaak R, Miller M and Hansen J 2007Europhys. Lett.7826002
- [7] E. Leutheusser, Phys. Rev. A29,2765 (1984)
- [8] W.Gotze and L.Sjogren,Rep.Prog.Phys.55,241(1992)
- [9] J.P. Hansen and I.R. McDonald, Theory of Simple Liquids (Elsevier, Amsterdam,2006).
- [10] C. A. Angell, Proc. Natl. Acad. Sci. 92, 6675 (1995)
- [11] D. Sidebottom and L. Torell, Phys.Rev. Lett.71, 2260(1993)
- [12] Fabbian, L., A. Latz, R. Schilling, F. Sciortino, P. Tartaglia, and C. Theis, Phys. Rev. E60, 5768 (1999).
- [13] Johari G P (1973) J. Chem. Phys.581766.
- [14] Biroli, G.; Bouchaud, J.-P. The Random First-Order Transition Theory of Glasses: A Critical Assessment; arXiv:0912.2542, (2009).
- [15] T. R. Kirkpatrick and D. Thirumalai, arXiv:1412.5017 (2014).
- [16] J.P. Bouchaud,G. Biroli,J. Chem. Phys. 121, 7347 (2004).
- [17] R. Richert,C. A. Angell,: J. Chem. Phys. 108, 9016 (1998).
- [18] L.Berthier,W. Kob,Phys.Rev.E011102 (2012) 2–6
- [19] Montanari, A. & Semerjian, G. J Stat Phys (2006) 125: 23. <https://doi.org/10.1007/s10955-006-9175-y>
- [20] G. Adam and J. W. Gibbs, J. Chem. Phys.43,139 (1965).
- [21] Frenkel, D.; Smit, B. Understanding Molecular Simulation from Algorithms to Applications; Academic Press: San Diego, CA, 2002.
- [22] G. Biroli, J. Bouchaud, A. Cavagna, T. Grigera, and P.Verrocchio,Nature Phys.4, 771 (2008).

- [23] Grigera, T. S. & Parisi, G. Fast Monte Carlo algorithm for supercooled soft spheres. *Phys. Rev. E* 63, 045102 (2001).
- [24] Li, Y., Mascagni, M., & Gorin, A. *Parallel Computing*, 35, 269 (2009).
- [25] Garcia, A., H. Herce, and D. Paschek. 2006. Simulations of temperature and pressure unfolding of peptides and proteins with replicaexchange molecular dynamics. *Annu. Rep. Comput. Chem.* 2:83–96.
- [26] Okabe, T.; Kawata, M.; Okamoto, Y.; Mikami, M. 2000, *Chem Phys Lett* 2001, 335, 435–439.
- [27] Biroli G., Karmakar S. and Procaccia I., *Phys. Rev. Lett.*, 111 (2013) 165701
- [28] M. P. Allen and D. J. Tildesley. *Computer Simulation of Liquids* (Oxford University Press, 1987).
- [29] G. M. Hocky, T. E. Markland, and D. R. Reichman, *Phys. Rev. Lett.* 108, 225506 (2012).
- [30] A. Cavagna, T. S. Grigera, and P. Verrocchio , *J. Chem. Phys.* 136, 204502 (2012)
- [31] Y. Kataoka and Y. Yamada, *J. Comput. Chem., Jpn.* 13, 257 (2014).